DEUTSCHES ELEKTRONEN-SYNCHROTRON DESY

DESY 79/85
December 1979

CHARACTERISTICS OF PHOTON-PHOTON INITIATED 3 JET EVENTS IN QCD

by

J. Field, E. Pietarinen
Deutsches Elektronen-Synchrotron DESY, Hamburg

K. Kajantie
Department of Theoretical Physics
University of Helsinki

NOTKESTRASSE 85 · 2 HAMBURG 52

To be sure that your preprints are promptly included in the
HIGH ENERGY PHYSICS INDEX ,
send them to the following address (if possible by air mail) :

DESY
Bibliothek
Notkestrasse 85
2 Hamburg 52
Germany

DESY 79/85
December 1979

Characteristics of photon-photon initiated 3 jet events in QCD

J.H. Field, E. Pietarinen

Deutsches Elektronen-Synchrotron DESY, Hamburg

K. Kajantie

Department of Theoretical Physics,

University of Helsinki

Abstract

The properties of photon-photon initiated 3-jet events of the type $e^+e^- \rightarrow e^+e^- qg(q\bar{q})$ + beam pipe jet are discussed. Expressions are derived in QCD for the total energy, longitudinal momentum and transverse momentum distributions of the beam pipe jet. These results are based on a generalization of Witten's result on photon structure functions to a distribution of two partons in a photon. The derivation is a novel application of jet calculus. The charge correlations typical of the 3 jet events are also analysed.

1. Introduction

The predictions of QCD in leading logarithm approximation for the jet structure arising from the photon-photon mechanism in very high energy e^+e^- collisions have recently been discussed in detail [1-5]. In photon-photon processes both the e^+ and e^- radiate an essentially parallel photon with a well-known Weizsäcker-Williams probability. In zeroth order of QCD the two photon collision leads to the production of a hadronic state of large p_T via the QED Born diagram shown in Fig. 1a. The high p_T of the two final state quarks ensures that the internal quark propagator is far from mass-shell giving a point like photon quark interaction which justifies use of perturbation theory. Higher order QCD diagrams leading to high p_T jets contain, in addition, a number of quarks and gluons nearly parallel with the initial direction for example that shown in Figs. 1b, 2a, where a quark and gluon recoil at large angles or in Fig. 2b where, as in the Born diagram, the jets come from $q\bar{q}$. These quarks and gluons form a small p_T jet, which we shall call the beam pipe jet. When all the diagrams are summed over [1,6-8], the cross sections of these 3 jet and 4 jet (containing 1 and 2, respectively, beam pipe jets) events can be expressed in terms of the distribution functions, calculable in QCD, of quarks and gluons in a photon (Fig. 2). Conversely, the QCD predictions can be tested by carrying out measurements on the 2 jet, 3 jet and 4 jet events.

The purpose of this paper is to consider the characteristics of 3 jet events; however the discussion can be easily extended to 4 jet events. A knowledge of the properties of the 3 jet events is clearly important for planning experiments on photon-photon initiated jets. To compare experiment with

the theoretical predictions, the 2, 3, 4 jet events must be separated. In particular, we shall discuss the properties of the beam pipe jet. Calculations so far have only pointed out its existence. Charge correlations will also be considered. The discussion of the angular width of the beam pipe jet will lead to a rather interesting novel application of jet calculus [9] to photons.

A clarification of the terms '3 jet event' and 'beam pipe jet' may be here in order. The physical basis for the existence of the third small-p_T jet in the processes of Fig. 2a, b is the following: The large p_T process probes the quark and gluon content of the electron with a quark of invariant mass $-q_T^2(1+e^{y_1-y_2})$. Before The invariant mass of the quark can attain this large value, the quark undergoes QCD evolution and emits further quarks and gluons. The relevant diagrams up to order α_s^2 are shown in Figs. 3a, b. The dominant configuration is one in which the produced quarks and gluons are nearly parallel with the incident electron. The object formed by these quarks and gluons or target fragments is in the following called the beam pipe jet. Strictly speaking, a 'jet' results from a single separated quark or gluon. Here we are extending this definition to include several almost collinear quanta. It is similar to the target fragmentation jet in deep inelastic leptoproduction.

In addition to the 3 jet events as defined above there are genuine 3 jet events obtained from QCD diagrams where more than one propagator is hard. In Fig. 4 the $q\bar{q}g$ diagram with two hard propagators leads to a genuine 3 jet event. The angles between the quanta remain constant when $s \to \infty$ and the cross section is calculable from the lowest order diagram

without the need for a leading log summation. Processes of this type have been considered in connection with hadron-hadron scattering in [10].

On the theoretical level, the basic object we shall consider in the following is $f_{a_1 a_2|\gamma}(x_1, x_2, Q^2, \mu^2)$, the double longitudinal inclusive probability density of finding two quanta ($a_{1,2} = q,g$) in a photon (Fig. 5). Here a_2 is the q or g initiating the hard collision, a_1 is another jet originating from the photon. The mass of a_2 is of the order of Q^2, that of a_1 of the order of μ^2. The distribution $f_{a_1 a_2|\gamma}$ generalizes in a natural way the photon structure function $f_{a|\gamma}$ derived by Witten [6]. Its derivation is a new application of jet calculus [9]. One of the properties of $f_{a_1 a_2|\gamma}$ is the energy momentum sum rule

$$\sum_{a_1} \int_0^1 dx_1\, x_1 f_{a_1 a_2|\gamma}(x_1, x_2, Q^2, \mu^2) = (1-x_2) f_{a_2|\gamma}(x_2, Q^2, \mu^2) \qquad (1)$$

which expresses the fact that the expectation value of the scaled energy of the fragmentation jet a_1 added to the scaled energy x_2 of the hard quantum a_2 gives 1. To determine the energy distribution of the beam pipe jet (section 2) we only need $f_{a_2|\gamma}$.

2. The beam pipe jet in photon-photon initiated 3 jet processes

We shall in this section first discuss the beam pipe jet in the valence approximation, i.e., assuming that QCD evolution takes place only via gluon radiation from quarks. This leads to more transparent formulas and is also likely to be a good approximation to the complete QCD evolution

result (section 3).

The cross section for the 3 jet event in Fig. 1b producing two large p_T jets at (y_1, q_T) and $(y_2, -q_T)$ is (for a u quark) given by

$$\frac{d\sigma}{dy_1 dy_2 d^2q_T} = x_1 f_{\gamma/e}(x_1)\, x_2 f_{u/e}(x_2)\, \frac{1}{\pi}\, \frac{d\hat{\sigma}^{\gamma u\to gu}}{d\hat{t}} \tag{2}$$

where

$$\frac{d\hat{\sigma}^{\gamma u\to gu}}{d\hat{t}} = \frac{4}{3}\, \frac{2\pi\alpha\alpha_s e_u^2}{\hat{s}^2}\left(\frac{\hat{s}}{-\hat{u}} + \frac{-\hat{u}}{\hat{s}}\right) \tag{3}$$

$$x_1 = \frac{1}{2}x_T(e^{y_1}+e^{y_2}),\quad x_2 = \frac{1}{2}x_T(e^{-y_1}+e^{-y_2}),\quad x_T = 2q_T/\sqrt{s} \tag{4}$$
$$\hat{s} = x_1 x_2 s,\quad \hat{t} = -\tfrac{1}{4}s x_T^2(1+e^{y_2-y_1}),\quad \hat{u} = -\tfrac{1}{4}s x_T^2(1+e^{y_1-y_2})$$

$$f_{\gamma/e}(x) = \frac{\alpha}{2\pi}\log\frac{s}{4m_e^2}\,\frac{1+(1-x)^2}{x} \tag{5}$$

and

$$f_{u/e}(x_2,Q^2,\mu^2) = \int_0^1 d\bar{x}\,d\bar{z}\,\delta(x_2-\bar{x}\bar{z})\, f_{u/\gamma}(\bar{z},Q^2,\mu^2)\, f_{\gamma/e}(\bar{x})$$
$$= \int_0^1 d\bar{x}\,dz\,dw_2\, f_{\gamma/e}(\bar{x})\left[z^2+(1-z)^2\right]\delta(x_2-\bar{x}zw_2)\cdot \tag{6}$$
$$\frac{3e_u^2\alpha}{2\pi}\int_{\mu^2}^{Q^2}\frac{dp^2}{p^2}\, f_{u/u}(w_2,Q^2,p^2)$$

where, in standard notation, the x^{n-1}-moments of $f_{u/u}$ are

$$f^n_{u/u}(Q^2,p^2) = \left[\frac{\alpha_s(Q^2)}{\alpha_s(p^2)}\right]^{d_n^{qq}} \tag{7}$$

To sum over $\frac{1}{2}n_f$ flavour doublets, Eq. (2) is to be multiplied by $n_f(1 + 1/16)$.

To describe the beam pipe jet we calculate the distribution in the variables z_B, x_B and p_T^2, defined as follows:

(1) z_B is the scaled momentum of the valence quark within the beam pipe jet.

(2) x_B is the scaled momentum of the whole beam pipe jet, i.e., adding the contributions of the fragmentation leg and the hard process leg in Fig. 1(b), $x_B = \bar{x}(1-z) + \bar{x}z(1-w_2) = \bar{x} - \bar{x}zw_2 = \bar{x} - x_2$. This is simply energy conservation. Note that $z_B = x_B$ if $w_1 = w_2 = 1$, i.e., no gluon radiation takes place (Born approximation). In general $z_B + x_2 < \bar{x} < 1$.

(3) p_T^2 is the transverse momentum of the fragmentation leg in Fig. 1(b), which in the present valence approximation is the same as the p_T of the whole beam pipe jet. The transverse momentum p_{TV} of valence quark within the beam pipe would be given by $p_{TV} = w_1 p_T$ since its momentum is reduced by w_1 due to gluon bremsstrahlung.

The calculation of the distribution in x_B is very simple: including $\delta(x_B - \bar{x} + x_2)$ one has

$$\frac{d}{dx_B} f_{q/e}(x_2) = f_{q/\gamma}\left(\frac{x_2}{x_2+x_B}\right) f_{\gamma/e}(x_2+x_B)\,\Theta(1-x_2-x_B)/(x_2+x_B) \tag{8}$$

which is to be inserted to Eq. (2). To calculate the distribution in z_B we need the two-parton distribution in a photon (Eq. (1)). In the present valence approximation the z_B distribution is given by evaluating the jet calculus diagram in Fig. 1(b) and is obtained from Eq. (2) by replacing there $\int_{u|e}(x_2)$ by $\int_{u\bar{u}|e}(x_2, z_B)$:

$$\int_{u\bar{u}|e}(x_2,z_B,Q^2,\mu^2) = \int_0^1 d\bar{x}\,dz\,dw_2\,dw_1\,\delta(x_2-\bar{x}zw_2)\times$$
$$\delta(z_B-\bar{x}(1-z)w_1)\int_{\gamma|e}(\bar{x})\frac{3e_u^2\alpha}{2\pi}\left[z^2+(1-z)^2\right]\int_{\mu^2}^{Q^2}\frac{dp^2}{p^2}\int_{u|u}(w_2,Q^2,p^2)\int_{\bar{u}|\bar{u}}(w_1,p^2,\mu^2) \tag{9}$$

Since the valence quark distribution is normalized we also have

$$\int_0^1 dz_B \int_{u\bar{u}|e}(x_2,z_B,Q^2,\mu^2) = \int_{u|e}(x_2,Q^2,\mu^2) \tag{10}$$

The p_T^2 distribution is calculated by changing the integration variable p^2 in (9) to p_T^2. For a process $q = p_1 + p_2$ with $E_1 + p_{1L} = z(q_0 + q_L)$ the exact general kinematic relation is

$$q^2 = \frac{p_1^2}{z} + \frac{p_2^2}{1-z} + \frac{p_T^2}{z(1-z)} \tag{11}$$

In agreement with the rules of jet calculus [9] we have in Eq. (9) assumed that $|p_1^2| = p_2^2 = p^2$. Since $q^2 = 0$ Eq. (11) then implies that $dp^2/p^2 = dp_T^2/p_T^2$. The consequences of the assumption $|p_1^2| = p_2^2$ clearly deserve further study, here, as well as in jet calculus in general.

As the distribution in the total energy x_B of the beam pipe jet can be expressed in terms of the known structure functions $\int_{a|\gamma}(x,Q^2)$, a = u,d,g we also give here the general result, not assuming the validity of the valence approximation. Now also the two subprocesses $\gamma q \to gq$ and $\gamma g \to q\bar{q}$ (Fig. 2) contribute:

$$\frac{d\sigma}{dy_1 dy_2 d^2q_T dx_B} = \left(\frac{\alpha}{2\pi}\log\frac{s}{4m_e^2}\right)^2 \frac{\alpha^2}{q_T^4}\,\frac{1}{(1+\cosh Y)^2}\,\underline{\bar{X}} \tag{12}$$

where ($Y = y_1 - y_2$)

$$\underline{\bar{X}}^{\gamma q} = \frac{64}{9}\,\frac{n_f}{33-2n_f}\left[1+(1-x_1)^2\right]\left[U(x_B,x_2)+\frac{1}{4}D(x_B,x_2)\right]\left(1+e^{-Y}+\frac{1}{1+e^{-Y}}\right) \tag{13}$$

$$\underline{\bar{X}}^{\gamma g} = \frac{16}{3}\,\frac{n_f}{33-2n_f}\left[1+(1-x_1)^2\right]G(x_B,x_2)\cosh Y \tag{14}$$

Here U, D and G are given by (cf. Eq. (8))

$$A(x_B,x_2) = \int_A\left(\frac{x_2}{x_B+x_2}\right)\frac{1}{2}\,\frac{1+(1-x_B-x_2)^2}{x_B+x_2}\,\theta(1-x_B-x_2), \qquad A = U,D,G \tag{15}$$

where

$$\int_A(x) = x\int_{A|\gamma}(x,Q^2)\Big/\frac{\alpha}{\pi}\log Q^2, \qquad A = u,d,g \tag{16}$$

is the Q^2-independent part of the distribution of an $e_q = \frac{2}{3}$(u), $e_q = -\frac{1}{3}$(d) quark or a gluon (g). For numerical purposes we shall use the simple parametrizations [4]:

$$f_u(x) = 0.16\ (x + \tfrac{1}{2})$$
$$f_d(x) = 0.03\ (x + 1) \qquad (17)$$
$$f_g(x) = 0.174x^{-0.6}(1-x)$$

E.g., $f_u(x)$ above differs from the exact result by less than 5 % for $0.05 < x < 0.95$. A more detailed parametrization can be found in [11]. In the Born approximation

$$U^B(x_B, x_2) = \frac{1}{3} x_2 (x_2^2 + x_B^2) \frac{1+(1-x_B-x_2)^2}{(x_B+x_2)^4} \theta(1-x_B-x_2) \qquad (18)$$
$$D^B = \frac{1}{4} U^B, \quad G^B = 0$$

Note also that since the aim is to discuss the beam pipe jet, Eqs. (13)-(14) only include the processes where the e^- turns to a quark or gluon which collide with a photon from the e^+. If the direction of the e^+ is defined as the positive longitudinal direction, the beam pipe jet will then go to the negative direction. Also, the form of the Y-dependent factor in (13) is such that it corresponds to $y_1(y_2)$ being the gluon (quark) rapidity, i.e. the gluon prefers to go to the negative direction. The rates of 3 jet processes in which the roles of e^+ and e^- are interchanged are simply obtained by permuting $y_i \to -y_i$.

To give numerical predictions we choose $\sqrt{S}$ = 200 GeV, n_f = 4 and fix the

hard process so that the two large p_T jets are both at 90°, $y_1 = y_2 = 0$ (also $y_1 = y_2 = 2$; jets at 15° to the beams)and let x_T have the value 0.1, q_T = 20 GeV (also x_T = 0.2, 0.4).

Numerical examples of the distribution in the total energy x_B of the beam pipe jet given by Eqs. (12)-(17) are shown in Figs. 6-7. We can draw following conclusions from these figures:

- the beam pipe jet has a rather broad energy distribution. In fact, the distribution $d6/dx_B$ does vanish at $x_B \to 0$ for both of the subprocesses shown in Figs. 6-7, but this is not evident for $\gamma q \to gq$ due to the approximate parametrization (17) used for $f_{q/\gamma}$. Actually $f_{q/\gamma} \to 0$ when $x \to 1$ like $1/\log(1-x)$, the turnover being at $x \simeq 0.9$.

- the $\gamma q \to gq$ subprocess dominates over $\gamma g \to q\bar{q}$ at small x_B while the latter is large at x_B near its maximum value $1 - x_2$. This reflects (Eq. (17)) the different behaviour of the quark and gluon distribution functions $f_{q|\gamma}(x)$ and $f_{g|\gamma}(x)$: the former dominates at x near 1.

- the peaking at small x_B is stronger for large y_1 and y_2 since $x_2 = \frac{1}{2}x_T(e^{-y_1} + e^{-y_2})$ is small then.

- the Born approximation alone gives a good estimate of the overall situation.

Predictions calculated on the basis of Eq. (9) (with $dp^2/p^2 = dp_T^2/p_T^2$)

are shown in Figs. 8-10. The calculation is carried out by straightforward numerical integration using Eqs. (2), (6) and (9). The distributions in p_T^2, p_{TV}^2, x_B and z_B are obtained by substituting suitable δ-functions under the integral signs.

3. The distribution of two partons in a photon

Eq. (9) gives the distribution of a u and $\bar{u}$ quark in an electron (or photon) in the valence approximation. To calculate the full QCD expression for $f_{a_1 a_2 | \gamma}(x_1, x_2, Q^2)$ we use the fact that the photon couples to quarks only via the pointlike $\gamma \to q\bar{q}$ coupling and let the two quark lines evolve and branch to give the two partons a_1 and a_2. The sum of all the contributions can be expressed in terms of the two jet calculus diagrams of Fig. 5. In the calculation of diagram (1) one has to integrate over the invariant mass p^2 of the q coupling to the photon. This integral can be written in the following alternative forms:

$$\int_{\mu^2}^{Q^2} \frac{dp^2}{p^2} \frac{\alpha}{2\pi} = \int_0^Y dy \frac{\alpha}{\alpha_s(p^2)} = \int_{\mu^2}^{Q^2} \frac{dp_T^2}{p_T^2} \frac{\alpha}{2\pi} \tag{19}$$

where p_T ($p_T^2 \approx -p^2$) is the relative transverse momentum of a_1 and a_2 (see remarks after Eq. (10)) and

$$Y = \frac{1}{2\pi b} \log \frac{\alpha_s(\mu^2)}{\alpha_s(Q^2)}, \quad y = \frac{1}{2\pi b} \log \frac{\alpha_s(\mu^2)}{\alpha_s(p^2)} \tag{20}$$

In the following we use (Y, Q^2) or $(y, p^2$ or $p_T^2)$ interchangeably. Y,y defined by eq. (20) should be discriminated from the rapidity variables. The result is then (as a slight generalization of Eq. (9))

$$f^{(1)}_{a_1 a_2 | \gamma}(x_1, x_2, Y) = 3 \sum_1^{2n_f} e_q^2 \int_0^Y dy \frac{\alpha}{\alpha_s(p^2)} \int_0^1 dz dw_1 dw_2 \delta(x_2 - w_2 z) \times$$

$$\delta(x_1 - w_1(1-z)) f_{a_1 | \bar{q}}(w_1, y) f_{a_2 | q}(w_2, Y-y) P_{q\bar{q}|\gamma}(z) \tag{21}$$

where

$$P_{q\bar{q}|\gamma}(z) = z^2 + (1-z)^2 \tag{22}$$

and $f_{a_1|\bar{q}}$ and $f_{a_2|q}$ describe the evolution of a quark from the scale p^2 (to be integrated over) to the scales μ^2 and Q^2, respectively. Equivalently, in terms of x^{n-1} moments we can write:

$$f^{(1)}_{a_1 a_2 | \gamma}(n_1, n_2, Y) = 3 \sum e_q^2 \int_0^Y dy \frac{\alpha}{\alpha(p^2)} f_{a_1|q}(n_1, y) f_{a_2|q}(n_2, Y-y) P_{q\bar{q}|\gamma}(n_1, n_2) \tag{23}$$

where

$$P_{q\bar{q}|\gamma}(n_1, n_2) = B(n_1+2, n_2) + B(n_1, n_2+2) \tag{24}$$

To discuss the p_T dependence one may replace y in (21) by p_T^2 using (19) with the result (y also contains p_T^2 via (20))

$$f^{(1)}_{a_1 a_2 | \gamma}(x_1, x_2, Q^2, p_T^2) = 3 \sum e_q^2 \frac{\alpha}{2\pi} \frac{1}{p_T^2} \int_{x_2}^{1-x_1} dz \left(\frac{z}{1-z} + \frac{1-z}{z} \right) \times$$

$$f_{a_1|q}\left(\frac{x_1}{1-z}, y\right) f_{a_2|q}\left(\frac{x_2}{z}, Y-y\right) \tag{25}$$

For the diagram (2) in Fig. 5 one similarly obtains

$$\delta^{(2)}_{a_1a_2|\gamma}(n_1,n_2,\Upsilon) = 3\sum e_q^2 \int_0^\Upsilon dy \frac{\alpha}{\alpha(p^2)} P_{q|\gamma}(n_1+n_2-1) \int_{a_1a_2|\gamma}(n_1,n_2,\Upsilon-y) \tag{26}$$

$$= 3\sum e_q^2 \int_0^\Upsilon dy \frac{\alpha}{\alpha(p^2)} \int_y^\Upsilon dy' \int_{a_1|b_1}(n_1,y') \int_{a_2|b_2}(n_2,\Upsilon-y') P_{b_1b_2|j}(n_1,n_2) \times$$

$$\int_{j|q}(n_1+n_2-1, y'-y)\, P_{q|\gamma}(n_1+n_2-1) \tag{27}$$

where

$$y' = \frac{1}{2\pi b} \log \frac{\alpha(\mu^2)}{\alpha(k^2)} \tag{28}$$

$$P_{q|\gamma}(n) = \int_0^1 dx\, x^{n-1}\left[x^2+(1-x)^2\right] = \frac{1}{n} - \frac{2}{n+1} + \frac{2}{n+2} \tag{29}$$

and $P_{b_1b_2|j}(n_1,n_2)$ is the double moment of the b_1b_2j vertex. The complete result for the distribution of two partons in a photon is given by the sum of Eqs. (21) and (27). Since $\int_{a|b}(n,y)$ is a matrix exponential function in y, the integrations in (21) and (27) are easily carried out. However, the result is rather lengthy and will not be presented here.

The necessity and sufficiency of the two diagrams is made obvious by checking the energy-momentum sum rule (1), which in terms of moments, gives

$$\sum_{a_1} \int_{a_1a_2|\gamma}(2,n_2,\Upsilon) = \int_{a_2|\gamma}(n_2,\Upsilon) - \int_{a_2|\gamma}(n_2+1,\Upsilon) \tag{30}$$

where [1,6]

$$\int_{a|\gamma}(n,\Upsilon) = 3\sum e_q^2 \int_0^\Upsilon dy \frac{\alpha}{\alpha(p^2)} \int_{a|q}(n,\Upsilon-y) P_{q|\gamma}(n) \tag{31}$$

is the moment of the single parton distribution function (see eq. (21) below). Eq. (30) for the sum of Eqs. (21) and (27) follows simply from the fact that the building blocks of Eqs. (21) and (27) also satisfy energy momentum sum rules.

To understand the behaviour of $\int_{a_1a_2|\gamma}(x_1,x_2,\Upsilon)$ analytically we shall only consider the diagram (1) in Fig. 5 in valence approximation, i.e. including only gluon emission in the evolution of the quark line. Experience with $\int_{a|\gamma}(x,\Upsilon)$ [2] indicates that this is a good approximation for values of $x \gtrsim 0.2$. For smaller x there is anyway the uncertainty arising from the phenomenological vector meson contribution arising from the direct $\gamma \to V$ coupling. Also one may note that the diagrams contributing to the jet calculus diagram (2) in Fig. 5 are at least of the order α_s^2 while diagram (1) starts with α_s^0 .

In the valence approximation

$$\int_{a|q}(n,\Upsilon) = \delta_{aq}\left[\frac{\alpha_s(Q^2)}{\alpha_s(\mu^2)}\right]^{d_n} \tag{32}$$

where d_n is the standard non-singlet anomalous dimension satisfying

$$d_1 = 0, \qquad d_n \underset{n\to\infty}{\to} \frac{C_F}{\pi b}\left[\log n - \left(\frac{3}{4} - \gamma\right)\right] = A\log n - B \tag{33}$$

Then

$$\int^{V}_{\bar{q}q|\gamma}(n_1,n_2,Q^2) = \int^{B}_{\bar{q}q|\gamma}(n_1,n_2,Q^2)\,\frac{1}{1+d_{n_2}-d_{n_1}}\left[\left(\frac{\alpha_s(Q^2)}{\alpha_s(\mu^2)}\right)^{d_{n_1}} - \left(\frac{\alpha_s(Q^2)}{\alpha_s(\mu^2)}\right)^{1+d_{n_2}}\right] \tag{34}$$

where $\int^{B}_{\bar{q}q|\gamma}$ is the double moment of the Born approximation (summed over $u,\bar{u},d,\bar{d},\ldots$):

$$\int^{B}_{\bar{q}q|\gamma}(n_1,n_2,Q^2) = 3\sum e_q^2\,\frac{\alpha}{2\pi}\log Q^2\left[B(n_1+2,n_2)+B(n_1,n_2+2)\right] \tag{35}$$

Note that the valence approximation to $\int_{a|\gamma}(n,\gamma)$ is obtained from (34) by putting $d_{n_1} = 0$. Then the last term $(\log\mu^2/\log Q^2)^{1+d_{n_2}}$ can be asymptotically neglected and the only Q^2 dependence of the result is a multiplicative factor $\log Q^2$ as in the Born approximation. However, in Eq. (34) both terms have to be taken into account even at large Q^2.

The p_T^2 dependence of the result is most conveniently analysed by starting from Eq. (25). Consider further the limit $1-x_1-x_2 \to 0$, in which the valence approximation should be applicable. Then one can use in the integrand the $x \to 1$ limit of the valence quark distribution in a quark (cf. Eqs. (32)-(33)):

$$\int_{q|q}(x,\gamma) = \frac{e^{\left(\frac{3}{4}-\gamma\right)2C_F\gamma}}{\Gamma(2C_F\gamma)}\,(1-x)^{2C_F\gamma-1} \tag{36}$$

Inserting this into (25) one obtains, in the limit $1-x_1-x_2 \to 0$,

$$\int^{(1)}_{\bar{q}q|\gamma}(x_1,x_2,Q^2,p_T^2) = 3\sum e_q^2\,\frac{\alpha}{2\pi}\,\frac{e^{\left(\frac{3}{4}-\gamma\right)2C_F\gamma}}{\Gamma(2C_F\gamma)}(1-x_1-x_2)^{2C_F\gamma-1}\times$$
$$(x_1^2+x_2^2)\,\frac{1}{p_T^2}\left[\frac{\alpha_s(p_T^2)}{\alpha_s(Q^2)}\right]^{\frac{C_F}{\pi b}\log\frac{1}{x_2}}\left[\frac{\alpha_s(\mu^2)}{\alpha_s(p_T^2)}\right]^{\frac{C_F}{\pi b}\log\frac{1}{x_1}} \tag{37}$$

This is to be compared with the Born approximation

$$\int^{B}_{q\bar{q}|\gamma}(x_1,x_2,Q^2,p_T^2) = 3\sum e_q^2\,\frac{\alpha}{2\pi}\,\delta(1-x_1-x_2)(x_1^2+x_2^2)\,\frac{1}{p_T^2} \tag{38}$$

Eq. (37) can be used to make a rough estimate of the rates of e^+e^- $e^+e^- q_V g + (BPJ \to \bar{q}_V(z_B,p_T^2))$ in place of the numerical evaluation of Eq. (9). The comparison of (37) and (38) shows the modification of the two parton structure function due to gluon radiation.

4. Charge Correlations

When the hard scattering process leading to the 3 jet topology is $\gamma q \to g q$ (Fig. 1b) the beam jet carries charge opposite to that of the high p_T quark jet. Denoting the electric charges of the two high p_T elementary quanta, gluon and quark by Q_1 and Q_2 and that of the beam pipe jet by Q_B the

following charge correlations may be defined:

$$C_1 = \langle Q_1 Q_2 \rangle$$
$$C_2 = \langle Q_B (Q_1 + Q_2) \rangle \qquad (39)$$

As the gluon is neutral $Q_1 = 0$ so for this subprocess

$$C_1 = 0 \qquad (40)$$

and $C_2 = \langle Q_B Q_2 \rangle$

The value of C_2 may be found by averaging over quark flavours. From Fig. 1b it can be seen that the cross section is weighted by the 4th power of the quark charge. In the case that both the 2/3 and 1/3 charge members of a given quark generation are above threshold C_2 has the value: $\left[(2/3)^4(-4/9) + (1/3)^4(-1/9)\right] / \left[(2/3)^4 + (1/3)^4\right] = -\frac{65}{153}$ independent of the number of generations. Between thresholds, if the charge 1/3 member of the generation is lighter, C_2 will be smaller than this, the difference becoming smaller as the number of generations increases. For example, well above the $b\bar{b}$ threshold, but below the $t\bar{t}$ one (5 flavours excited) the expected value of C_1 is $\frac{-131}{315}$ differing from the constant 'even flavour' value by only 2 %.

Because of the neutrality of the photon and the gluon Q_B is expected to be zero in 3 jet events originating from $\gamma g \to q\bar{q}$ (Fig. 2b). For the same reason $Q_1 = -Q_2$ in this case. This implies that:

$$C_1 = -\langle e_q^2 \rangle \qquad (41)$$

the weighting factor for the different flavours now being e_q^2, while

$$C_2 = 0. \qquad (42)$$

For excitation of any number of complete quark generations

$$C_1 = \left[\left(\frac{2}{3}\right)^2\left(-\frac{4}{9}\right) + \left(\frac{1}{3}\right)^2\left(-\frac{1}{9}\right)\right] / \left[\left(\frac{2}{3}\right)^2 + \left(\frac{1}{3}\right)^2\right] = -\frac{17}{45} \qquad (43)$$

The charge correlations expected for the two different subprocesses are thus strikingly different. For a kinematic configuration such as that shown in Fig. 7, where the relative contributions of the two sub-processes change strongly as a function of x_B, a similarly large change in the charge correlation coefficients C_1, C_2 is also to be expected. In practise, of course, the charge of the elementary quantum must be estimated from that of the leading $z \to 1$ hadrons in the jet, the dilution of the elementary charge correlation, resulting from this depending on the details of the fragmentation mechanism. After the completion of this paper we noted that charge correlations in $\gamma\gamma$ collisions have also recently been studied by Soni [12].

Acknowledgements

K.K. thanks the DESY theory group for hospitality. E.P. acknowledges the support by the Academy of Finland.

Figure Captions

Fig. 1 (a) the 2 jet process, (b) the 3 jet process $e^+e^- \to e^+e^- qg$ + beam pipe jet. y_i are the lab rapidities of the high p_T quanta. x_1, x_2 are scaled momenta of the photon, quark participating in the hard collision. $\bar{x}$ and z_B are scaled momenta of the other photon and the valence quark within the beam pipe jet. z, w_1 and w_2 are momentum branching fractions as indicated by the arrows. Q^2 and p^2 indicate the off shell mass scales of the hard and intermediate partons.

Fig. 2 The two subprocesses in 3 jet processes (a) $\gamma q \to g q$ and (b) $\gamma q \to q \bar{q}$

Fig. 3 Generation of the beam pipe jet in the course of QCD evolution

Fig. 4 A $\gamma\gamma$ process leading to three genuine non-degenerate jets

Fig. 5 The jet calculus diagrams contributing to $\int a_1 a_2 |_\gamma (x_1, x_2, \bar{Q}^2)$

Fig. 6 The distribution of the total energy x_B of the beam pipe jet at $\sqrt{S}$ = 140 GeV for values of variables marked on the figure.

Fig. 7 As Fig. 6 but at $y_1 = y_2 = 2$

Fig. 8 The distribution of the p_T^2 of the beam pipe jet for values of variables marked on the figure.

Fig. 9 The distribution of the p_T of the valence quark within the beam pipe jet for various values of its longitudinal momentum

Fig. 10 The distribution of the momentum fraction z_B of the valence quark within the beam pipe jet for x_T = 0.2 and 0.4.

References

1 C. Llewellyn Smith, Phys. Lett. 79B (1978) 83

2 S.J. Brodsky, T. DeGrand, J. Gunion and J. Weis, Phys. Rev. Lett. 41 (1978) and Phys. Rev. D19 (1979) 1418

3 K. Kajantie, Physica Scripta 29 (1979) 230 and University of Helsinki preprint HU-TFT-79-5, 1979, Acta Phys. Austriaca, Suppl. XXI (1979) 663

4 K. Kajantie and Risto Raitio, University of Helsinki preprint HU-TFT-79-13, and Nucl. Phys. B159 (1979) 528

5 M. Abud, R. Gatto and C.A. Savoy, University of Geneva preprint UGVA-DPT 1979/03-192

6 E. Witten, Nucl. Phys. B120 (1977) 189

7 W.R. Frazer and J.F. Gunion, Phys. Rev. D20 (1979) 147

8 W.A. Bardeen and A.J. Buras, Phys. Rev. D20 (1979) 166

9 K. Konishi, A. Ukawa and G. Veneziano, Phys. Lett. 78B (1978) 243 and Nucl. Phys. B157 (1979) 45

10 Z. Kunszt and E. Pietarinen, Nucl. Phys. B (in press), DESY preprint 79/34 T. Gottschalk and D. Sivers, Argonne preprint ANL-HEP-79-07

11 A. Nicolaidis, College de France preprint LPC 79-16, 1979

12 A. Soni, SLAC-PUB-2398 (1979), submitted to Phys. Rev.

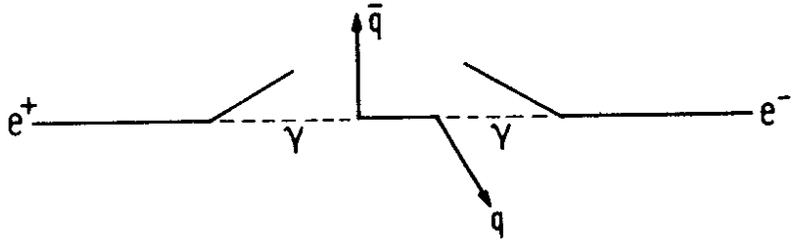

(a)

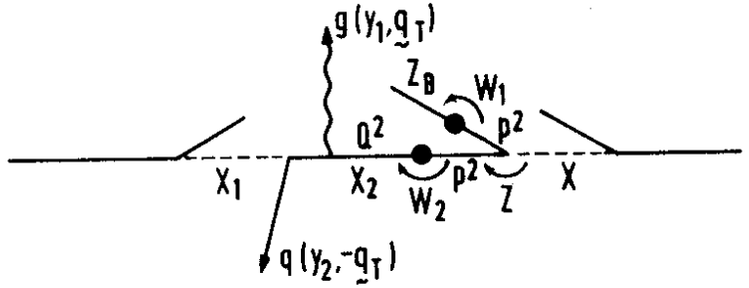

(b)

Fig. 1

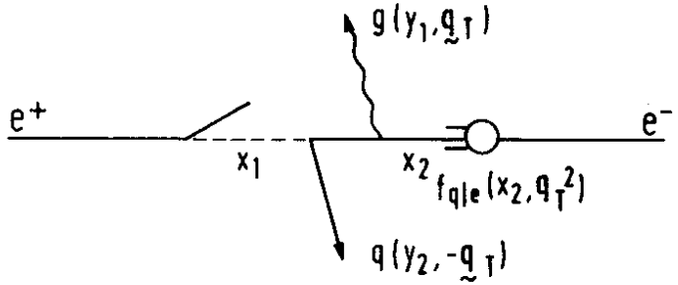

a)

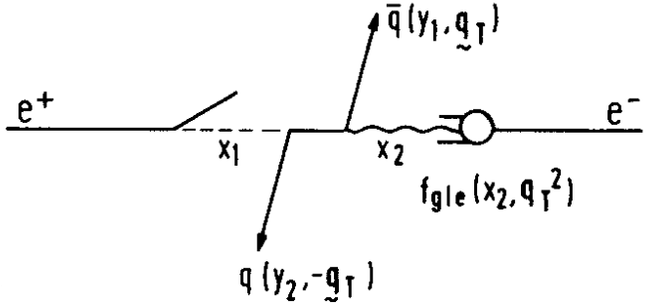

b)

Fig.2

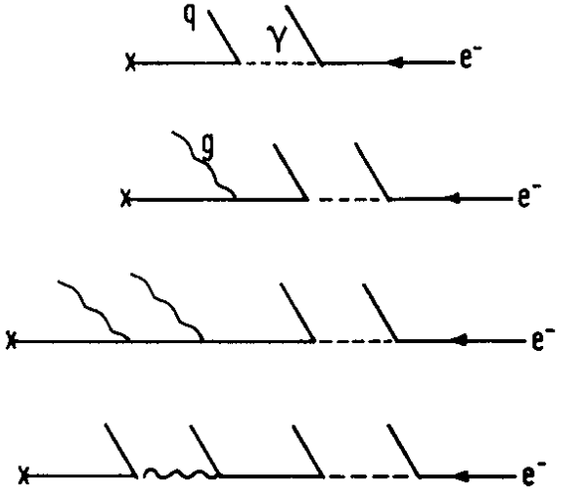

Fig.3a

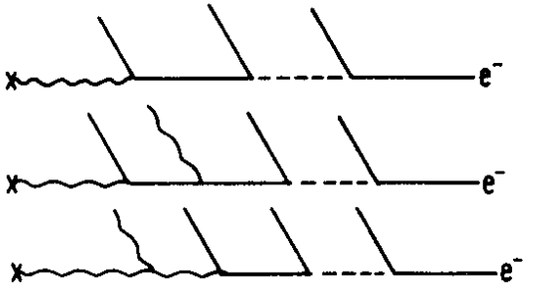

Fig.3b

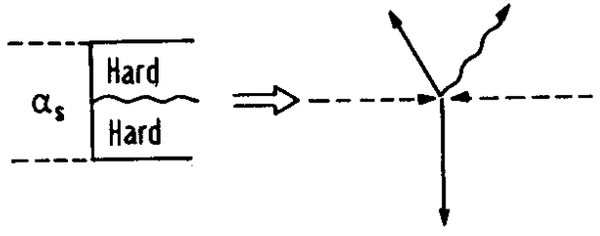

Fig. 4

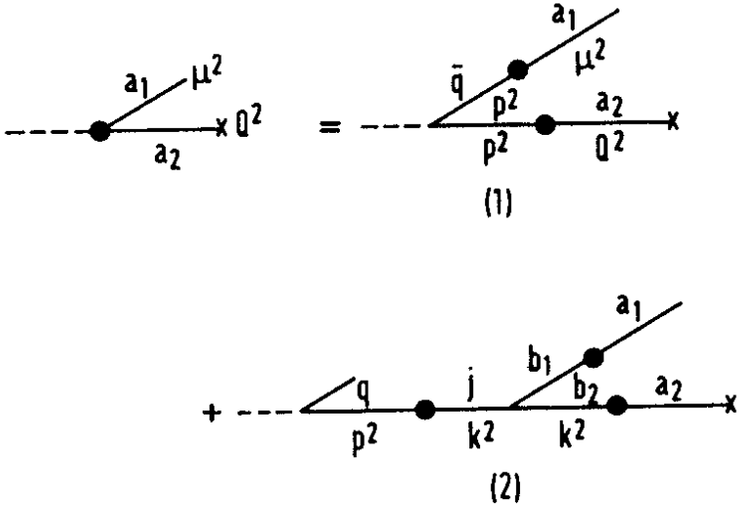

Fig. 5

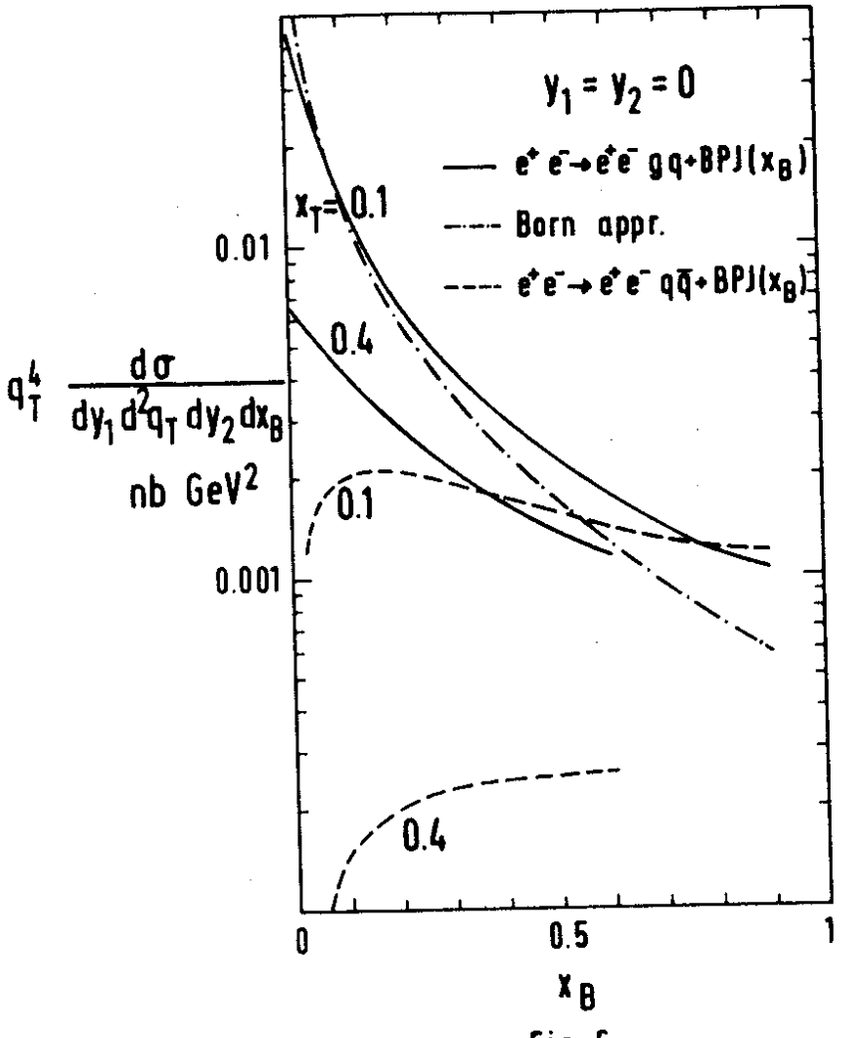

Fig. 6

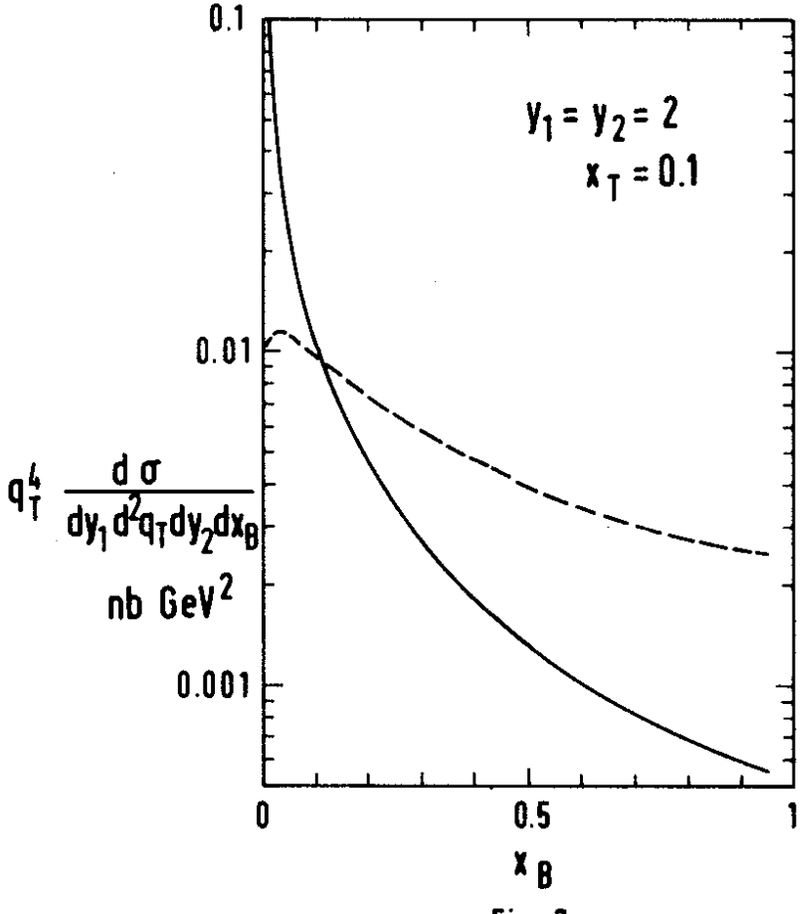
0.1
0.01
0.001
$y_1 = y_2 = 2$
$x_T = 0.1$
$q_T^4 \frac{d\sigma}{dy_1 d^2q_T dy_2 dx_B}$
nb GeV^2
0
0.5
1
x_B

Fig. 7

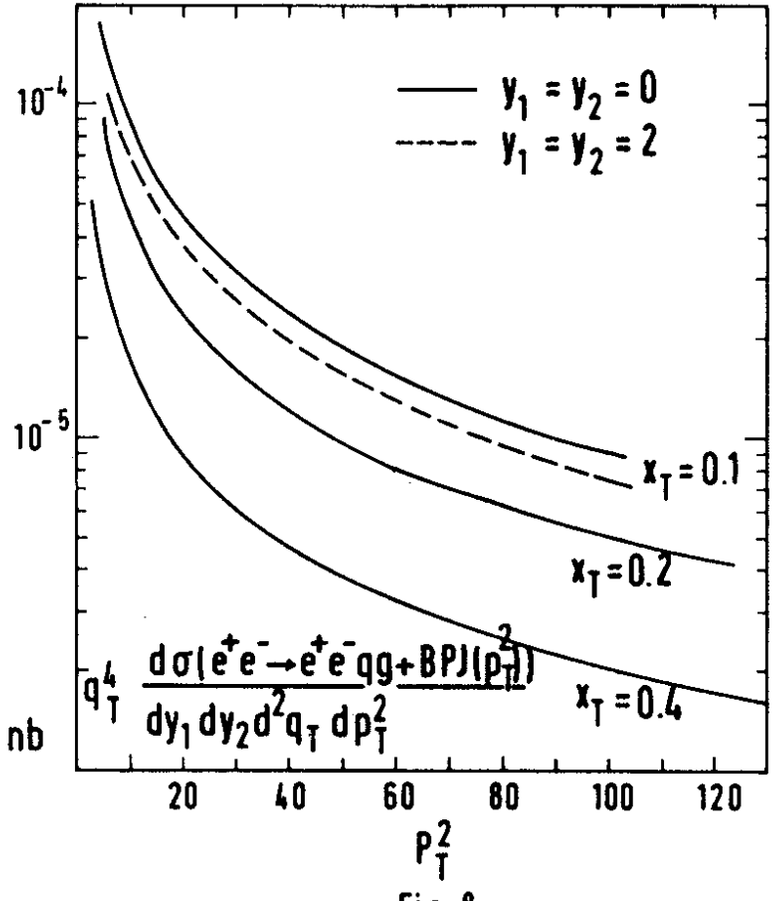
10^{-4}
10^{-5}
$y_1 = y_2 = 0$
$y_1 = y_2 = 2$
$x_T = 0.1$
$x_T = 0.2$
$x_T = 0.4$
$q_T^4 \frac{d\sigma(e^+e^- \to e^+e^- qg + BPJ(p_T^2))}{dy_1 dy_2 d^2q_T dp_T^2}$
nb
20
40
60
80
100
120
p_T^2

Fig. 8

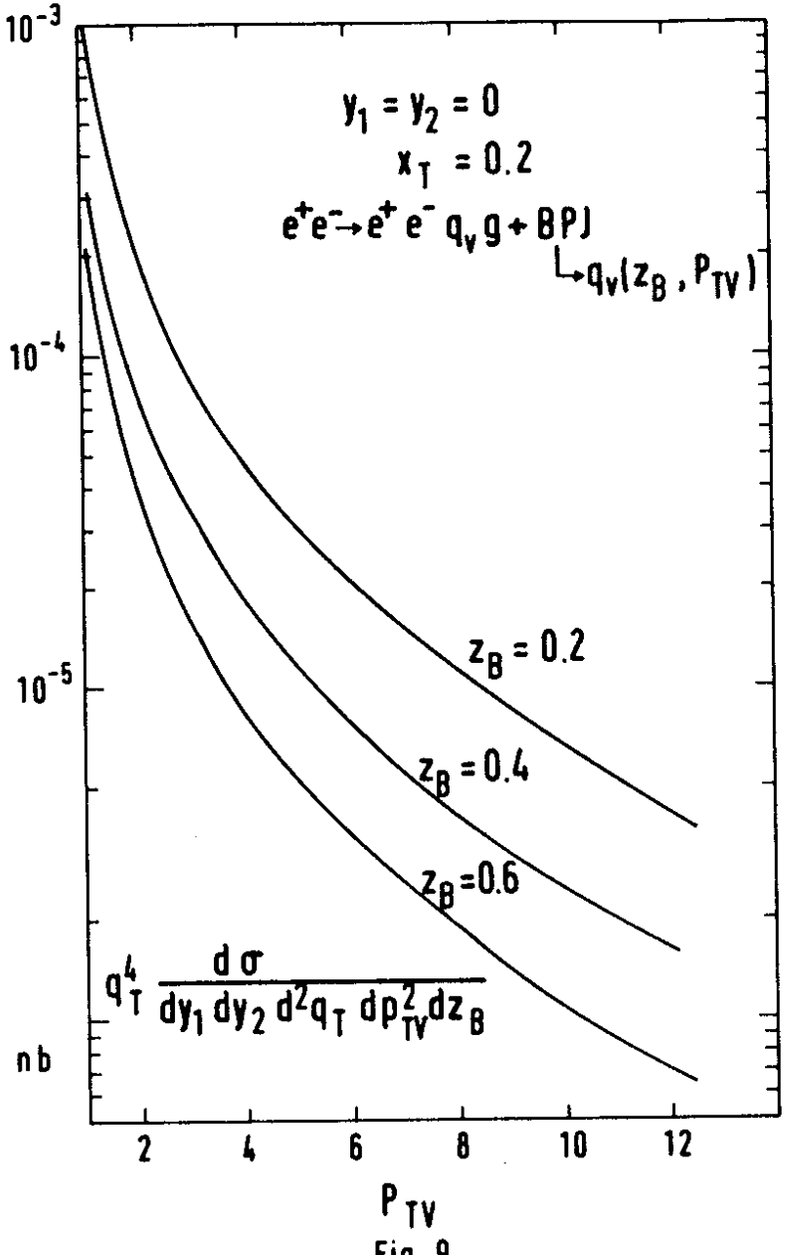
10^{-3}
10^{-4}
10^{-5}
nb
$y_1 = y_2 = 0$
$x_T = 0.2$
$e^+e^- \to e^+ e^- q_v g + BPJ$
$\hookrightarrow q_v(z_B, P_{TV})$
$z_B = 0.2$
$z_B = 0.4$
$z_B = 0.6$
$q_T^4 \frac{d\sigma}{dy_1 dy_2 d^2q_T dp_{TV}^2 dz_B}$
2
4
6
8
10
12
P_{TV}

Fig. 9

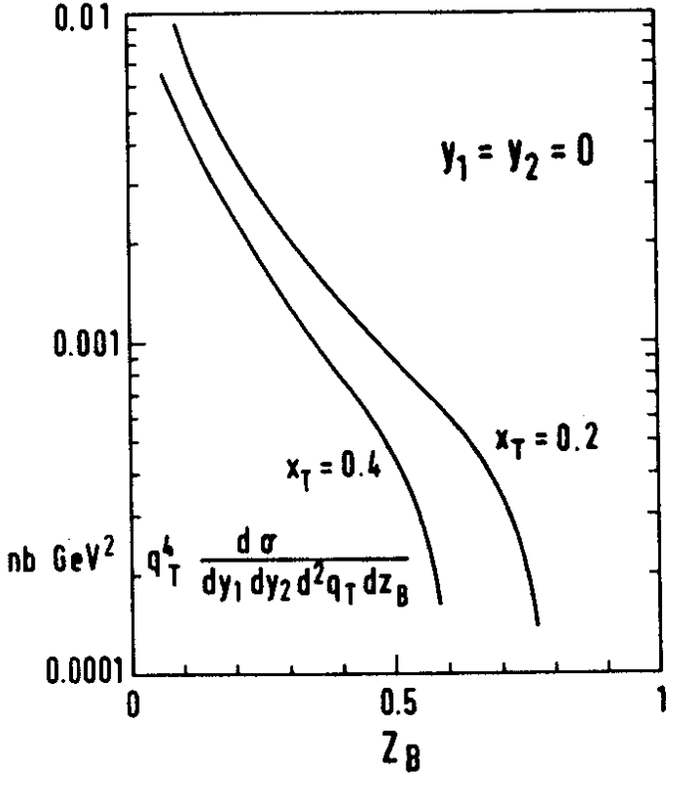
0.01
0.001
0.0001
nb GeV^2
$y_1 = y_2 = 0$
$x_T = 0.2$
$x_T = 0.4$
$q_T^4 \frac{d\sigma}{dy_1 dy_2 d^2q_T dz_B}$
0
0.5
1
Z_B

Fig. 10